Ocean Modelling 199 (2026) 102653

Contents lists available at ScienceDirect

Ocean Modelling

journal homepage: www.elsevier.com/locate/ocemod

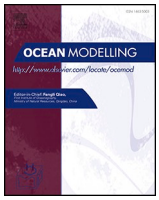

Assessing the effects of sea level rise on ocean waves and surge events along the victorian coast

Rui Li [a,*], Huy Quang Tran [a,b], Jak McCarroll [c], Alexander V. Babanin [a]

[a] Faculty of Engineering and Information Technology (FEIT), University of Melbourne, Melbourne, Victoria, Australia
[b] Stantec Australia, 600 Bourke Street, Melbourne, Victoria, Australia
[c] Biodiversity Division, Department of Energy, Environment and Climate Action (DEECA), Melbourne, Victoria, Australia

ARTICLE INFO

Keywords:
Sea level rise
Ocean wave
Storm surges
Hydrodynamics
SCHISM
WWMIII

ABSTRACT

This study investigates nonlinear surges and extreme wind-wave patterns off the coast of Victoria by simulating sea level rise (SLR) scenarios of 0.5, 0.8, 1.0 and 1.4 meters alongside a 31-year hindcast (1990–2020) using the validated SCHISM-WWMIII coupled wave-circulation model. Model simulations were compared with observational data, confirming the accuracy of the results. Our findings indicate that sea levels along the Victorian coast have been rising at a rate of 1.46×10^{-2} cm/year, while wave heights in the Southern Ocean have also increased over time. However, the rate of wave height increase is lower along the Victorian coast compared to the Southern Ocean. Due to island blocking, mean wave heights in Bass Strait remain lower than those in the Southern Ocean, yet extreme water levels in the strait exceed those in the open ocean. The impact of SLR is most pronounced in the waters south of Tasmania, where maximum elevations exceed 1.2 meters under the 1.0-meter SLR scenario. SLR contributes to higher mean water levels and increased wave heights off the coast of Victoria, underscoring the complex interactions between rising sea levels and coastal wave dynamics. Wave direction and peak period were also examined, but their changes under SLR scenarios were found to be minimal. These findings highlight the importance of incorporating both SLR and wave dynamics into coastal hazard assessments to better understand future risks.

1. Introduction

Understanding the interactions between waves and coastal hydrodynamics is essential for effective coastal management, operations, and resilience planning. Extreme sea levels and wind waves are key drivers of coastal dynamics, profoundly influencing natural ecosystems and human activities (Bhaskaran et al., 2022; Li et al. 2023; Wahl et al. 2017; Wright et al. 2020). Extreme sea levels, driven by storm surges, high tides, and sea level rise (SLR) due to climate change, can exacerbate coastal flooding and erosion, posing risks to infrastructure, water quality, and human populations. Similarly, extreme wind waves generated by intense storms contribute to sea-level variations and amplify coastal hazards, leading to further erosion, property damage, and threats to human safety (Dodet et al. 2019; Lyddon et al. 2019). These factors are critical in flood risk assessments, coastal management, and adaptation strategies.

The Southeast Australian seas are vital both oceanographically and socio-economically, hosting diverse ecosystems and some of Australia's most populous coastal cities, including Melbourne and Hobart (Morim et al. 2016). As key economic and cultural centers, these regions are highly vulnerable to coastal hazards. The wave climate is strongly influenced by the Southern Ocean, where intense westerly winds generate large swells that propagate northward, increasing significant wave height (SWH) and coastal erosion (Li et al. 2021; Li et al. 2022; Liu et al. 2021). The interaction of these swells with locally generated wind waves adds complexity to coastal dynamics, highlighting the need for detailed assessments under future SLR scenarios (Zhang et al. 2023c). Coupled wave-hydrodynamic modelling is essential for capturing these processes, providing valuable insights into wave transformation, coastal flood risks, and shoreline stability (Zhang et al. 2023a; Zhang et al. 2023b).

Previous studies have examined extreme sea levels and wind waves, including the work of (Hernaman et al. 2025; McInnes et al. 2009a; McInnes et al. 2009b; McInnes et al. 2013) and Tran et al (2023, 2024). McInnes et al. (2009a) investigated the effects of climate change on extreme sea levels in Port Phillip Bay (PPB) as part of a broader

* Corresponding author.
E-mail address: rui.li.4@unimelb.edu.au (R. Li).

https://doi.org/10.1016/j.ocemod.2025.102653
Received 16 May 2025; Received in revised form 28 October 2025; Accepted 13 November 2025
Available online 14 November 2025

assessment of Victoria's coastline. The study analyzed the influence of astronomical tides and storm events on storm surges, expressing extreme sea levels relative to mean sea levels, which were found to exceed storm surge heights. However, certain limitations exist, such as the use of a coarse computational grid that may not fully resolve complex topographic features in PPB. Additionally, the study did not account for wind-wave influences on storm surges, which could impact storm tide estimates due to wave-sea level interactions (Arns et al. 2020).

Recent studies (McInnes 2022; Tran et al. 2024) used the SCHISM–WWMIII model to assess SLR impacts in PPB, a semi-enclosed area less affected by Southern Ocean swells. This study expands the scope to the entire Victorian coastline and Tasmania, where both SLR and large-scale Southern Ocean climate modes shape coastal wave dynamics and water levels. Using updated wave physics (ST6) (Liu et al. 2019; Rogers et al. 2012) validated against observations, we simulate a 31-year hindcast (1990–2020) under multiple SLR scenarios. Our results also provide a high-resolution, statewide dataset that can support local-scale models of erosion, inundation, and shoreline change, as well as inform coastal planning and resilience efforts under climate change.

Estimating 50-year and 100-year return period elevation and SWH is also essential for coastal engineering, flood risk assessment, and infrastructure resilience (Kang et al. 2015; Li et al. 2023). These values help design seawalls, ports, and critical infrastructure to withstand extreme events. A 100-year return period is particularly important for long-term planning under climate change, as rising sea levels and intensifying storms may alter extreme event frequencies. By comparing historical and projected return levels, policymakers can develop adaptive strategies to protect coastal communities, minimize economic losses, and enhance disaster preparedness, ensuring sustainable coastal development in a changing climate.

The structure of this paper is as follows: Section 2 introduces the coupled SCHISM-WWM model and the observational data used for validation. Section 3 examines the hydrodynamic characteristics of the Southeast Australian seas at high resolution. Section 4 analyzes changes in SWH and water level under SLR scenario. Finally, Section 5 presents the conclusions and discussion.

2. Dataset and method

2.1. Numerical modelling frameworks

A coupled system combining a circulation model, and a wave model has been implemented to simulate the hydrodynamic conditions in Southeast Australian seas. This system is designed with high spatial resolution to accurately represent the complex coastal topography and bathymetry, utilizing the unstructured grid framework of SCHISM (Semi-implicit Cross-scale Hydroscience Integrated System), as described by Zhang and Baptista (Zhang and Baptista 2008; Zhang et al. 2016). SCHISM's key feature is its use of semi-implicit schemes to solve advection in the momentum equations, ensuring numerical stability and allowing for larger time steps (see Guérin et al. 2018). The system integrates directly with the spectral wave model WWMIII, which was developed by Roland (2008) and further refined by Roland et al.(2012). WWMIII is a third-generation, phase-averaged wave model based on an unstructured grid, designed to calculate wave spectra over both coastal and open ocean regions. From the computed spectral data, key wave parameters such as SWH, wave direction, and peak period can be derived. The WWMIII model solves the wave action balance equation, which incorporates various physical processes including wind energy input, white-capping dissipation, and bottom friction. WWMIII employs a residual distribution scheme to solve the geographical space, integrating features of both finite element and finite volume methods (Roland et al. 2012). The spectral space is solved using the UQ (Ultimate Quickest) method, similar to WW3 (Tolman 1992). Source terms are handled in three fractional steps: a third-order TVD (Total Variation Diminishing) Runge-Kutta method for dissipation terms (e.g., bottom friction, wave breaking), a dynamic scheme for nonlinear interactions (e.g., triads), and a semi-implicit scheme for deep-water source terms. This study utilizes the latest wave physics package (ST6) implemented in WWMIII by Tran(2020). Further details on the coupled model can be found in Section 2.1 of Tran et al.(2024) and are not repeated here.

2.2. Model setup

Given the complex coastal geometry and bathymetry along the Victoria and Tasmania waters, an unstructured grid framework is ideal as it provides flexibility in mesh size adjustments, effectively representing morphological features like irregular shorelines and complex bathymetry, especially at bay entrances. This approach also enhances the model's ability to capture ocean tides and waves from deep waters. Bathymetry data was interpolated onto the mesh using linear interpolation. The chosen mesh consists of 165,077 nodes and 309,855 elements, with resolution varying from approximately 20 m nearshore to 3 km offshore (see Fig. 1). The model domain extends from 140.0° E to 150.0° E and from 37° S to 45° S. The simulation was run with a computational time step of 240 s, and outputs were saved at hourly intervals.

2.3. Model forcing

Coastal models are generally used to simulate regions that interact with external areas through open boundaries, making it essential to define appropriate open boundary conditions. In coastal regions, tides and winds can cause significant water level fluctuations and currents, which can be particularly strong in areas like Port Phillip Heads. Coastal hydrodynamic models are often restricted to the open sea, known as the open boundary, where water levels fluctuate over time and space and must be specified. This study uses the global finite element solution tide model (FES 2014) developed by AVISO (Carrère et al. 2015) to specify water level variations at the open boundary. FES 2014 offers improved grid resolution, especially in coastal areas and continental shelves, using updated global bathymetry. It assimilates long-term altimeter data from sources such as Envisat, Topex/Poseidon, Jason-1, Jason-2, and tidal gauges. The FES 2014 database provides a resolution of 1/16°, which is 50 % finer than FES 2012. SCHISM was configured in a depth-averaged (2DH) barotropic mode, incorporating multiple tidal constituents (Z0, Q1, O1, P1, K1, N2, M2, S2, K2) based on FES 2014 data, produced by Noveltis, Legos, and CLS, and distributed by AVISO+ with CNES support (https://www.aviso.altimetry.fr/). Notably, the Z0 component represents a constant term describing the long-term mean state of SLR or fall. In this study, SLR was simulated by modifying the Z0 value in the model, specifically implementing 0.5, 0.8, 1.0 and 1.4 m increase at the open boundary with the phase set to zero.

Atmospheric forcing inputs for the SCHISM-WWM model were sourced from ERA5 reanalysis data (Hersbach et al. 2020). ERA5 is the fifth-generation atmospheric reanalysis from ECMWF, covering global climate from January 1940 to the present. Produced by the Copernicus Climate Change Service (C3S), ERA5 offers hourly estimates of various atmospheric, land, and oceanic variables on a 30 km grid, with 137 vertical levels extending from the surface to 80 km in height. For this study, atmospheric forcing includes 10 m wind speed, mean sea level pressure, 2 m air temperature, 2 m specific humidity, downward longwave and shortwave radiation fluxes, precipitation rate, all at sea level. The ERA5 hourly reanalysis data can be downloaded from https://cds.climate.copernicus.eu/datasets/reanalysis-era5-single-levels?tab=overview.

In the WWM wave model, ocean wave conditions are typically forced at the open boundary unless the computational domain is large or situated within a basin. Along the Victoria and Tasmania waters, waves from the Southern Ocean significantly influence local wave propagation. This study utilizes WW3 hindcast data from a wave hindcast conducted by the University of Melbourne (Liu et al. 2021), with a temporal resolution of 3 hours and a spatial resolution of 0.25°, including wave

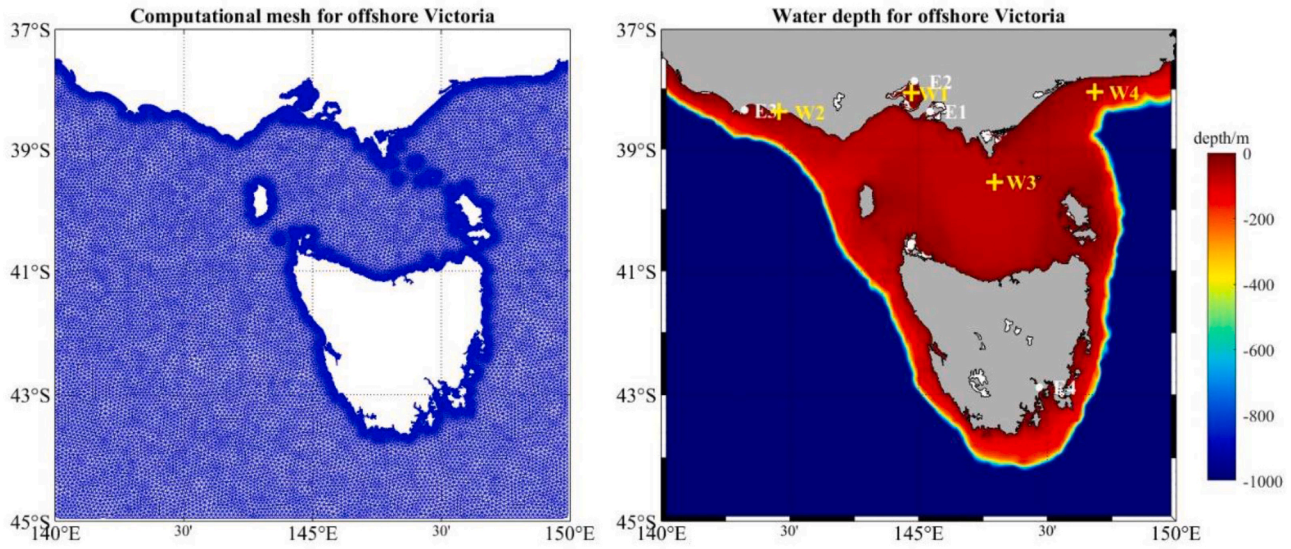

Fig. 1. Computational mesh and water depth used in this study. White dots indicate tide gauge stations, while yellow crosses represent wave buoys.

direction, peak frequency, SWH, directional spread, and mean period. What's more, several rivers discharge into the ocean within our study area; however, their influence was not included in the model configuration. Previous studies have shown that currents in this study area are predominantly driven by tides, and the influence of background ocean currents is relatively limited (Dong et al. 2025). Therefore, background currents and non-tidal residuals were not included in the boundary conditions. Details of other boundary conditions and model setup can be referred to in the work of Huy et al. (Tran 2020; Tran et al. 2023; Tran et al. 2024).

2.4. Observed data

There are several types of field measurements available along the Victoria waters. The Australian National Collection of Homogenised Observations of Relative Sea Level (ANCHORS) is a national sea level dataset based on tide gauge records across Australia (Hague et al. 2022). ANCHORS aims to monitor changes in mean sea level and coastal flood frequency around the country. It includes 38 tide gauge records, with record lengths ranging from 36 to 125 years, and an average duration of 59 years. Statistical homogenisation is applied to detect and correct non-geophysical shifts in the data, such as those caused by equipment upgrades or changes in tide gauge location. In this study, elevation observed data were sourced from four locations: Western Port, Melbourne, Portland, and Hobart, as shown in Table 1 and Fig. 1. The observed data can be downloaded from https://geonetwork.nci.org.au/geonetwork/srv/eng/catalog.search#/metadata/f2262_2926_6911_5843.

The Victorian Coastal Monitoring Program (VCMP) deployed SOFAR Spotter buoys along the Victoria coastline to monitor wave motions (Ierodiaconou et al. 2022). This real-time buoy network, part of a Victorian government initiative, aims to understand how deep-water waves transform as they approach the shore and to develop downscaled models that link wave climate to shoreline dynamics. The buoys, equipped with GPS positioning and satellite data transmission, record water surface fluctuations approximately every half second. The buoy locations include Port Fairy, Wilsons Prom, Lake Entrance, and Central PPB, and they measure wave variables such as SWH, peak direction, peak period, and mean period. The locations are shown in Table 2 and Fig. 1. The observed data can be downloaded from https://vicwaves.com.au/#.

2.5. Model calibration and validation

In a previous study, Tran et al. (2023) extensively calibrated and validated the model against various observed data in PPB. Therefore, this study expands beyond PPB to encompass the entire offshore region of Victoria. An initial two-month simulation (from 01/09/2021 to 01/11/2021) was performed, with the final month used to validate the SCHISM model and wave model against buoy observations. For the SCHISM model, elevation predictions were compared with observations, as shown in Figs. 2 and 3. The correlation was high at all four locations (>0.9) with a small positive bias (<0.1 m). Regardless of high or low tide conditions, the model results closely matched the observed elevation.

The same time period was selected to verify the wave results, as shown in Figs. 4 and 5. The correlation across all locations exceeds 0.9, indicating strong agreement between modeled and observed data. The normalized bias is less than 20 %, demonstrating the model's reliability in capturing SWH variations. The best model performance was observed at Wilsons Prom station. However, during large wave events, the model tends to overestimate SWH. In PPB, due to the terrain, SWH remain consistently below 3 m. The overestimation of SWH can be attributed to wave-current interactions and the presence of both swell and wind-sea, which pose challenges in wave modelling (Liu et al. 2021). However, DEECA (Department of Energy, Environment and Climate Action) prefers a slight overestimation rather than underestimation, especially when the results are used as input for local hazard assessment.

Overall, model data shows good agreement with the observed data.

Table 1
The locations of the four elevation observations.

Number	Tide Gauge Station	Longitude	Latitude
E1	Western Port	145.2228	−38.3739
E2	Melbourne	144.9165	−37.8657
E3	Portland	141.6197	−38.3514
E4	Hobart	147.3410	−42.8773

Table 2
The locations of the four wave buoys.

Number	Buoys Station	Longitude	Latitude
W1	Central PPB	144.8667	−38.0634
W2	Port Fairy	142.2879	−38.3817
W3	Wilsons Prom	146.4830	−39.5410
W4	Lake Entrance	148.4200	−38.0550

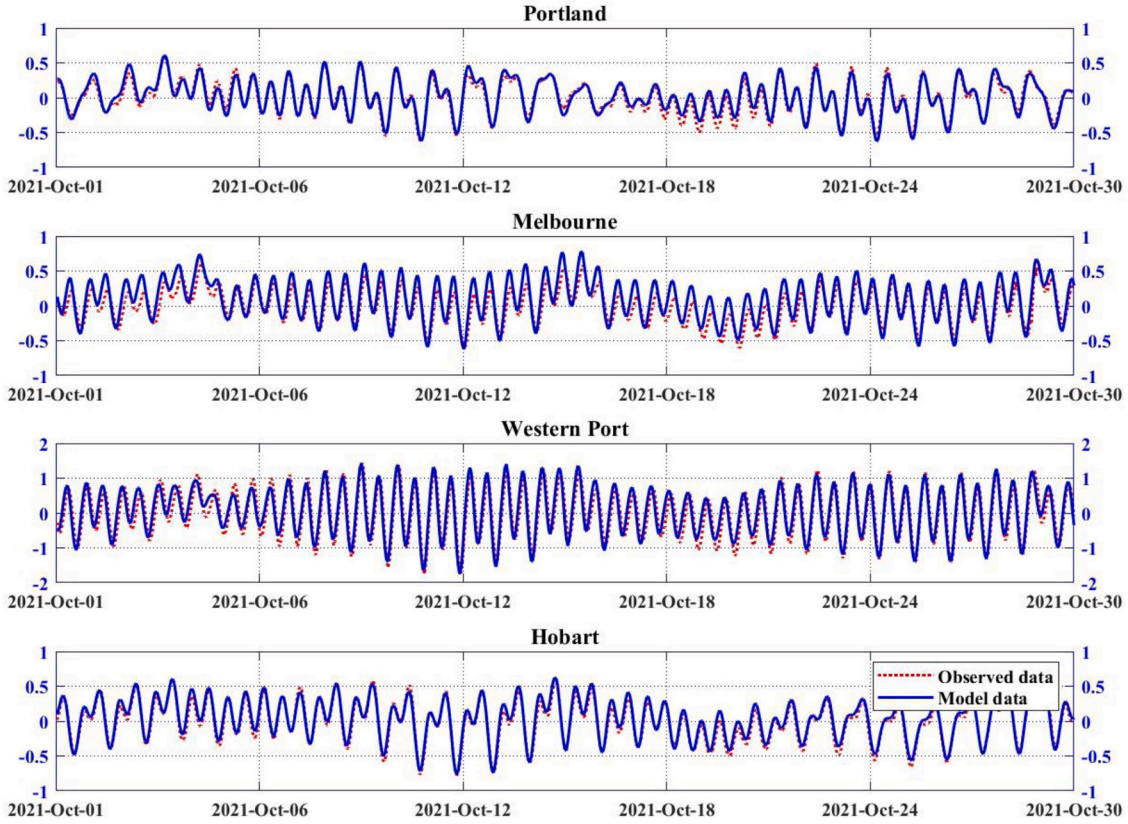

Fig. 2. Time series plots comparing modelled water levels against observed data for a period of one month (from 01/10/2021 to 29/10/2021).

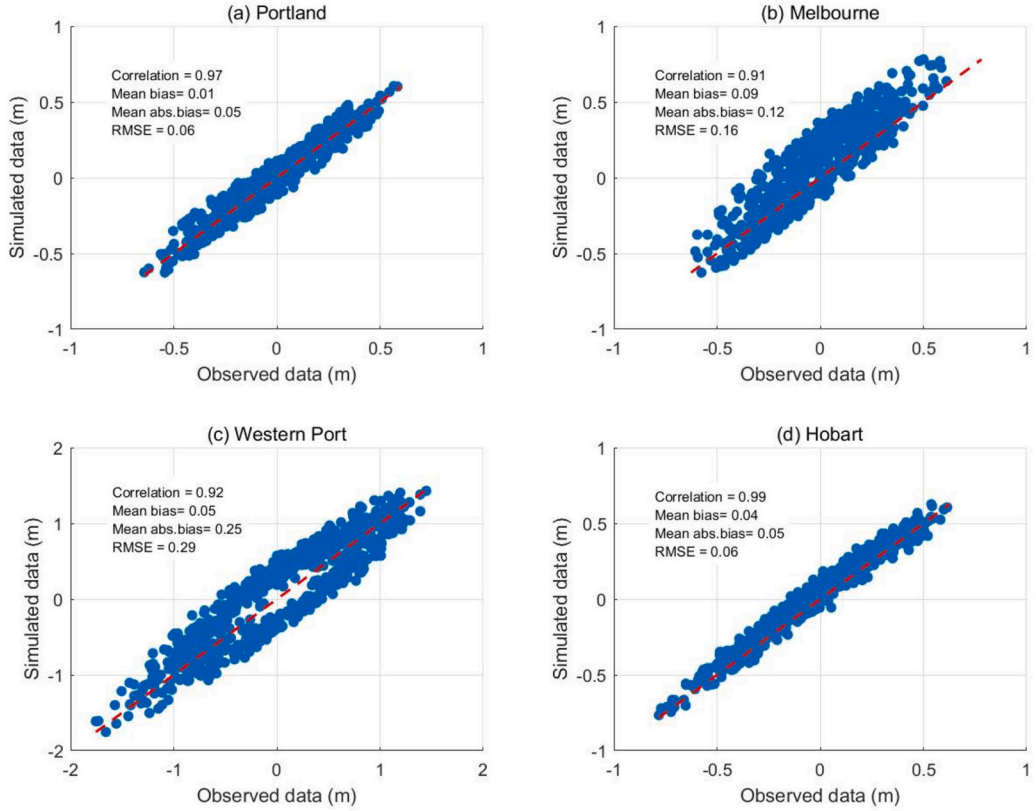

Fig. 3. Scatter plots showing the relationship between the modelled and observed elevation at four wave buoy locations (see Fig. 1 for locations) based on one month of data (from 01/10/2021 to 29/10/2021).

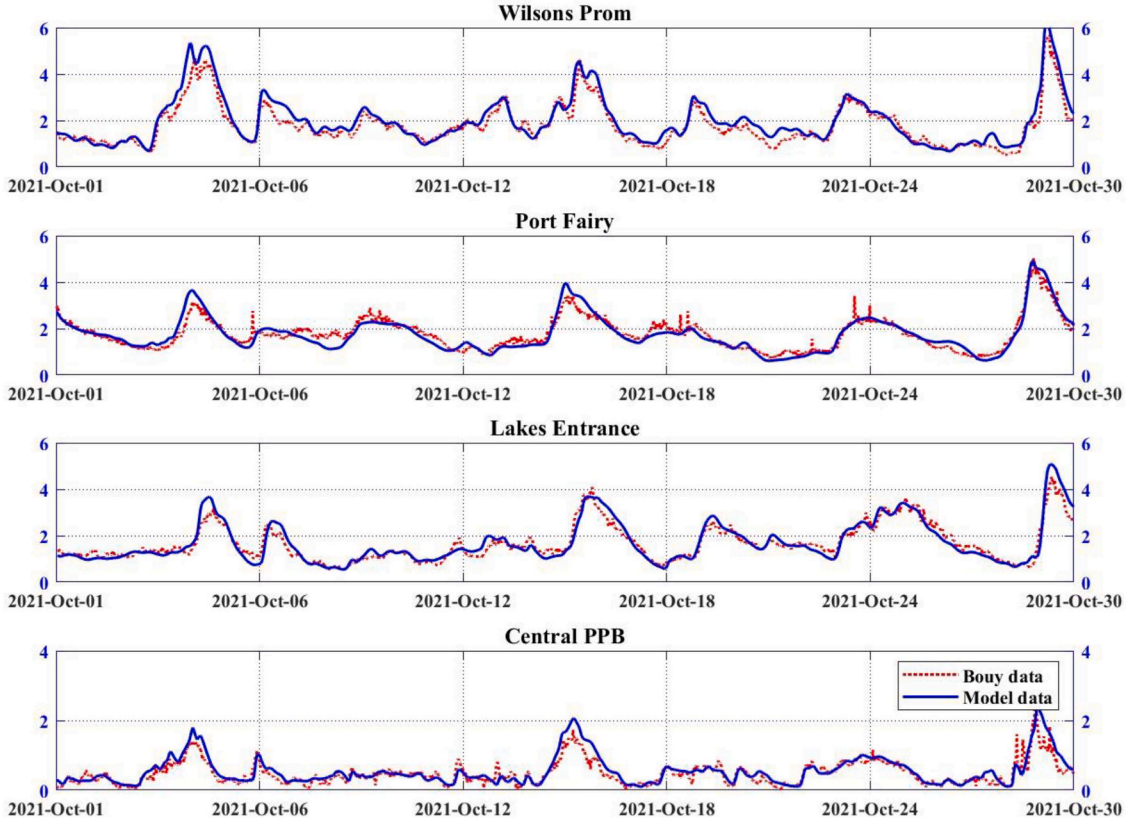

Fig. 4. Time series plots comparing modelled SWH against observed data for a period of one month (from 01/10/2021 to 29/10/2021).

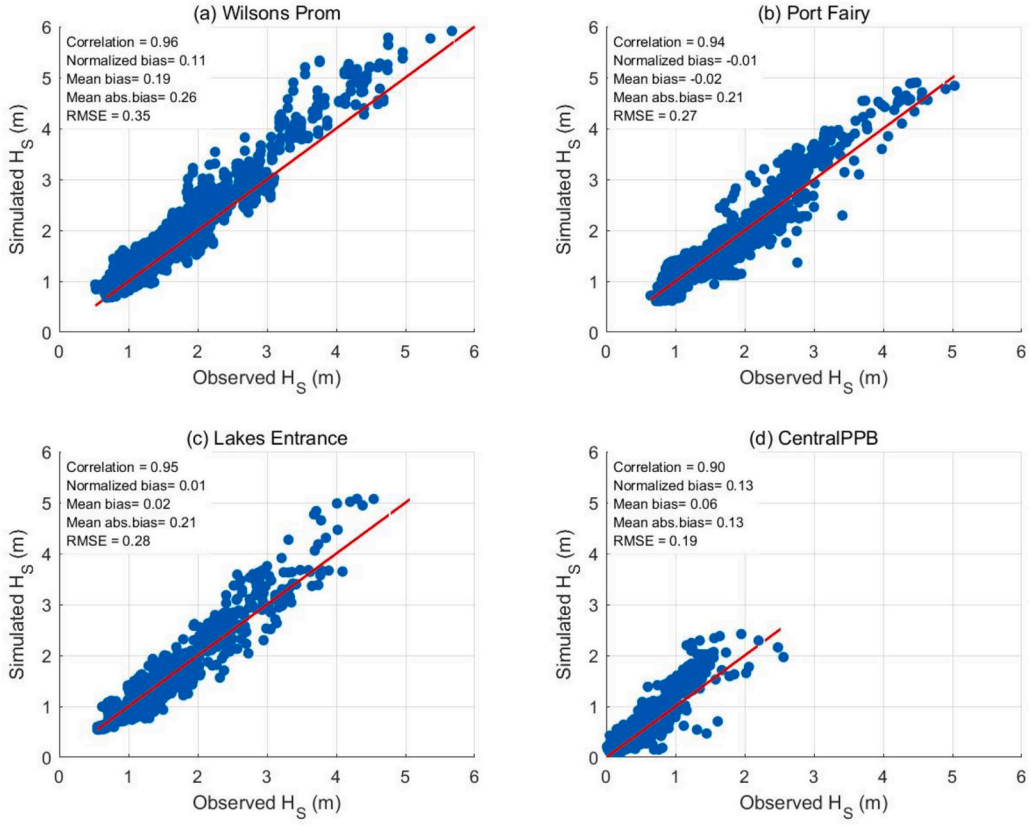

Fig. 5. Scatter plots showing the relationship between the modelled and observed SWH at four wave buoy locations (see Fig. 1 for locations) based on one month of data (from 01/10/2021 to 29/10/2021).

This model configuration was then used for hindcast, including in the different sea level scenarios. During model simulations, a one-month spin-up period was implemented to ensure stable initial conditions. The calculation time step was set to 240 s, with results output at hourly intervals.

2.6. The Gumbel distribution

Return values represent exceedance levels expected to occur on average once within a specified period. This study aims to estimate the return values of SWH and water level using statistical methods. Various approaches exist for this estimation. Woo and Park (2021) applied the peaks-over-threshold method to calculate 100-year return values. Fisher and Tippett (1928) introduced three extreme value distributions: Type III (Weibull), Type II (Fréchet), and Type I (Gumbel). Jenkinson (1955) and Coles(2001) later unified these into the Generalized Extreme Value (GEV) distribution, expressed as:

$$F(x) = \exp\left\{ -\left[1 + \frac{\gamma(x-\mu)}{\sigma}\right]^{-\frac{1}{\gamma}} \right\} \quad (1)$$

where $F(x)$ is the cumulative probability function, x is the variable, and γ, μ, and σ represent the shape, location, and scale parameters, respectively. When $\gamma = 0$, the GEV simplifies to the Gumbel distribution:

$$F(x) = e^{-e^{\frac{x-\mu}{\sigma}}} \quad (2)$$

The Gumbel distribution (Extreme Type I) is widely applied in hydrology and air pollution studies (Kochanek et al. 2014; Ercelebi and Toros 2009). Kang et al. (2015) and Li et al.(2023) used it to estimate extreme wind values and SWH values. The location and scale parameters can be determined through linear regression. Some previous studies (Anghel 2024; Jain 2011; Pryor and Barthelmie 2021) have shown that the Gumbel distribution provides stable and reasonable estimates for the annual maxima of wave heights and water levels. Its simpler form, with fewer parameters to estimate, helps reduce uncertainty, especially when the sample size is limited. Therefore, in this study, we adopt the Gumbel distribution (Eq. (2)) for extreme value estimation.

3. Existing extreme water level and ocean wave patterns

Before evaluating the impact of rising mean sea levels on extreme water levels and ocean waves, it is crucial to first establish their current patterns as a baseline for comparison. Fig. 6 illustrates the maximum and mean water levels and SWH across the study region based on hourly values. Due to the shielding effect of surrounding islands, SWH in Bass Strait are significantly lower than in offshore waters. This effect is most pronounced in the relatively enclosed PPB, where maximum SWH remain below 3 m, and mean SWH are less than 1 m

In contrast, along the Tasmanian coast, exposure to strong Southern Ocean wind fields and swells results in maximum SWH exceeding 10 m, with long-term averages around 4 m Water levels off the coast of Victoria show a gradual increase in both maximum and average values as they approach the shore, with PPB exhibiting the high water levels in the region. In particular, the maximum water level in PPB can exceed 1.4 m In Western Port Bay, the maximum water level is even higher, exceeding 2 m—significantly greater than the approximately 1.6 m observed in the surrounding open waters. Although the Bass Strait blocks the direct impact of Southern Ocean swells on the Victorian coast, it also contributes to maintaining relatively high water levels within the strait.

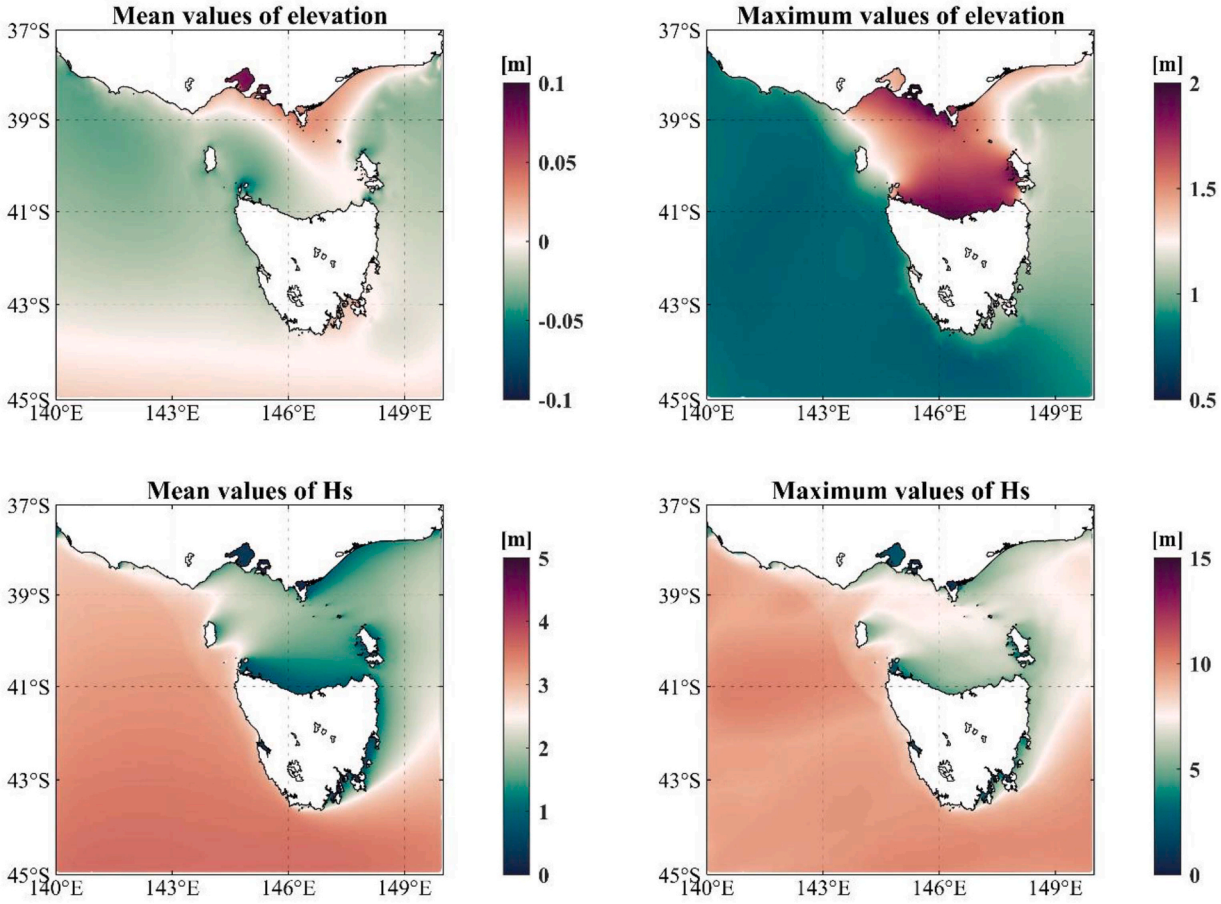

Fig. 6. Maximum and mean values of elevation and SWH over the 31 years, calculated from hourly values.

Despite experiencing the lowest SWH due to its enclosed geography, PPB consistently records the highest water levels, highlighting the complex interplay between topography and hydrodynamic processes.

Severe weather systems that generate extreme water levels and SWH pose significant risks to coastal infrastructure and management. To better understand these dynamics along the southeastern Australian coast, we analyzed the extreme elevations and SWH over a 31-year period. The calculation of 90th percentile (P90) and 99th percentile (P99) values is crucial, as these metrics help quantify the likelihood of extreme events, which is essential for coastal engineering design, flood risk assessment, and climate adaptation planning. By identifying regions more susceptible to extreme conditions, these statistics support the development of more resilient coastal management strategies in response to future sea-level rise and intensifying storm patterns. Fig. 7 presents the P90 and P99 values of SWH and water level, which provide key insights into the frequency and intensity of extreme events.

In PPB, the probability of the annual extreme water level exceeding 1.5 m is less than 1 %, while the probability of SWH exceeding 5.0 m is also below 1 %. A distinct spatial pattern emerges across Bass Strait, where SWH on the eastern side are generally lower than those on the western side due to the combined effects of bathymetry and wave direction (Liu et al. 2023). Additionally, the western and southern waters of Tasmania are consistently exposed to higher SWH, influenced not only by local wind waves but also by swell propagating from distant storms in the Southern Ocean (Liu et al. 2023).

The return levels for annual exceedance probabilities (AEP) of 1 % and 2 % were determined using extreme value analysis and computed across the entire model grid, as shown in Fig. 8. The spatial distribution of extreme water levels and SWH closely resembles the hindcast results. Extreme water levels are most pronounced in offshore Victoria, particularly in PPB, where the 50-year return level reaches approximately 1.5 m For extreme SWH, the 100-year return SWH in the Southern Ocean can reach up to 12 m Overall, the spatial patterns of return levels for both SWH and water level are consistent with those of the hindcasted extreme values.

With rising sea levels, Victoria's Resilient Coast: Adapting for 2100+ has recently adopted best-practice adaptation strategies (https://www.marineandcoasts.vic.gov.au/marine-coastal-management/victorias-resilient-coast-adapting-for-2100). These require consideration of multiple scenarios, incorporating a range of hazard event probabilities and sensitivity analyses for 2100 SLR projections, including 1.1 m and 1.4 m mean SLR. Their result—specifically, the estimated extreme water levels under these higher SLR scenarios—shows magnitudes comparable to the 100-year return period water levels along the Victorian coast presented in Fig. 8.

Regarding with the SWH in Southern Ocean, recent studies utilizing model datasets (Meucci et al. 2020; Sharmar et al. 2021) and altimeter observations, excluding CFSR-derived products, have identified extensive regions of significant increases in mean SWH, ranging from 1 to 3 cm per year, over the period from the 1980s to the 2010s (Young and Ribal 2019; Young et al. 2011). Based on the 31-year hindcast results, we also analyzed the long-term trends in water levels and SWH, as shown in Fig. 9. The findings indicate a persistent rise in sea levels off the coast of Victoria, particularly in PPB, where the increase reaches approximately 1.46×10^{-2} cm/year. This rate is lower than the observed global mean sea level rise, partly because the boundary conditions used in our model do not account for non-tidal residuals or large-scale background currents—such as storm surges or interannual variability—which can contribute to higher coastal water levels. While SWH in the Southern Ocean exhibit a noticeable upward trend, this is less pronounced in Bass Strait, especially within PPB. Our results align with previous studies, showing that SWH in the Southern Ocean can increase by up to 1 cm per year. Overall, while islands and topography can shield areas from wave influence, their impact on water levels is quite the opposite.

4. Potential changes in water level and wave height

The potential effects of SLR were assessed using 31-year hindcast data under four SLR scenarios: 0.5 m, 0.8 m, 1.0 m and 1.4 m. The

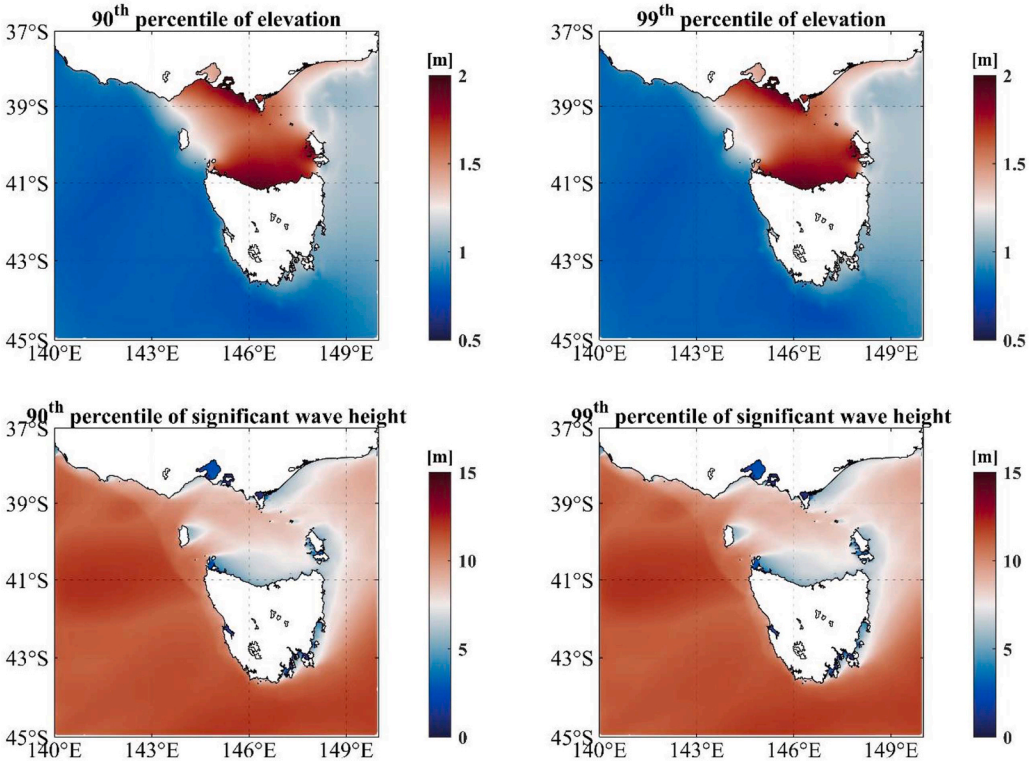

Fig. 7. P90 and P99 percentile elevation and SWH values over the 31 years based on extreme annual values.

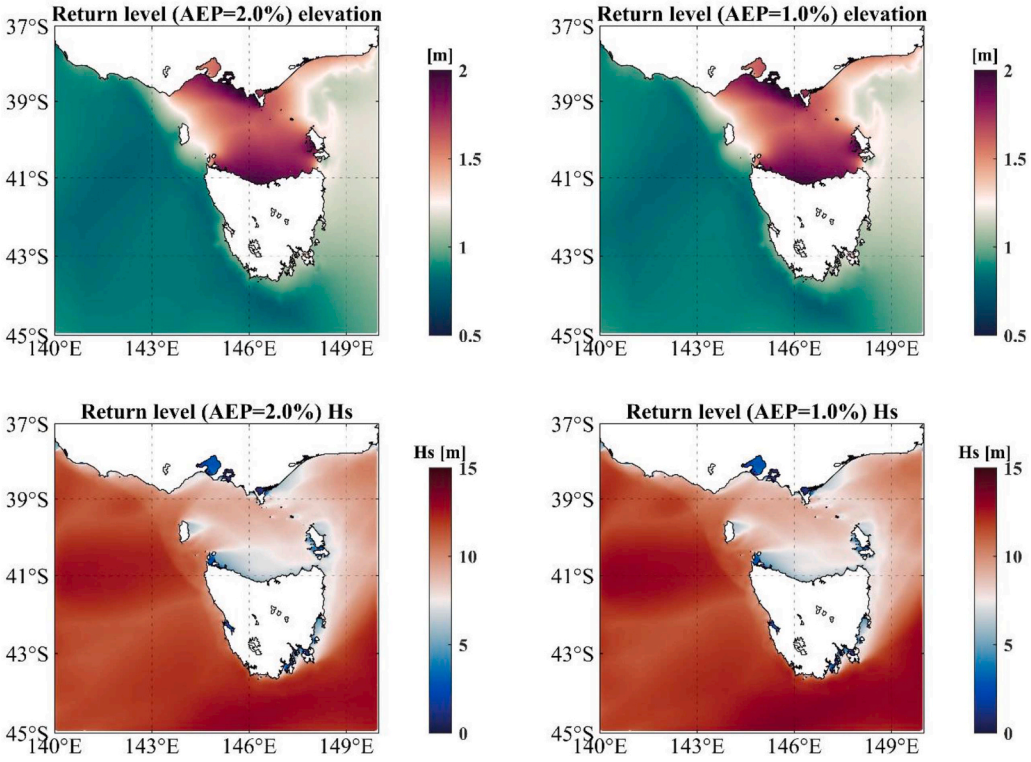

Fig. 8. Long-term return period values calculated with the Gumbel distribution method using the extreme annual values.

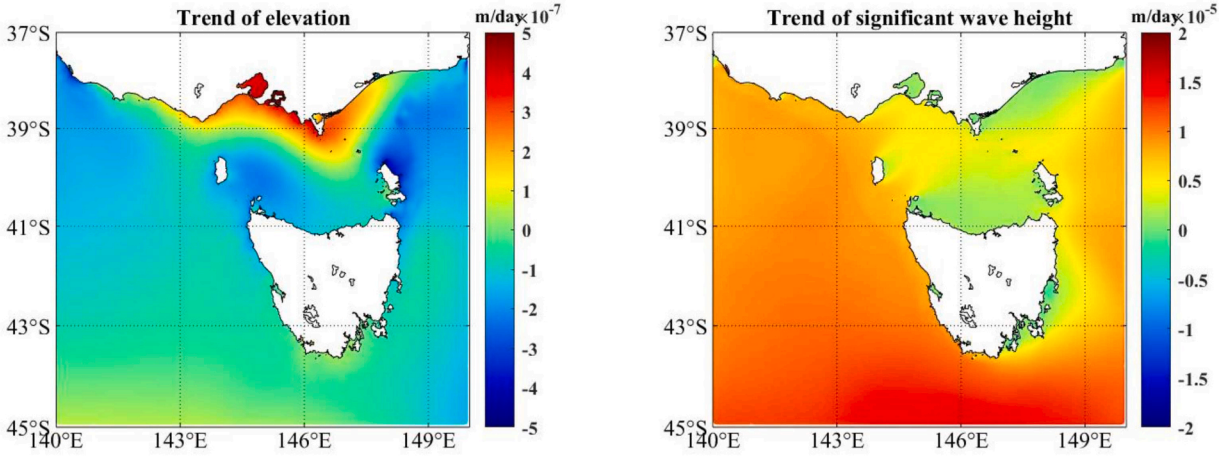

Fig. 9. Trends of elevation and SWH over the 31 years.

analysis evaluates changes in mean and maximum hourly values of water levels and SWH, providing insight into how these factors may respond under different SLR conditions. This approach helps to better understand the regional variability of extreme ocean conditions along the southeastern Australian coast.

Fig. 10 only shows the maximum and mean values of elevation and SWH under the 0.5-meter SLR scenario as a representative case. Including all scenarios would result in too many figures. The highest water levels occur along the Victorian coastline, particularly within PPB. Under a 0.5-meter SLR scenario, the maximum elevation in PPB remains around 2 m, while the mean elevation exceeds 0.5 m Notably, elevations in the southern and western Tasmanian seas also show substantial increases, with some regions exceeding 0.6 m These results indicate that SLR not only raises baseline sea levels but also amplifies mean water elevations, especially in semi-enclosed and low-energy coastal environments.

Across all four SLR scenarios, SWH changes remain relatively subtle compared to the results in Fig. 6. To better capture these variations, we computed the differences in mean elevation, maximum elevation, mean SWH, and maximum SWH between the four SLR scenarios and the baseline sea level. The results are presented in Figs. 11–14.

Under the 0.5-meter SLR scenario, the mean elevation increases by approximately 0.6 m in the southern Tasmanian Sea, while under the 1.0-meter SLR scenario, increases of up to 1.1 m are observed in some regions (Fig. 11). Although different SLR scenarios were applied, the spatial variability remains consistent, with the largest increases concentrated south of Tasmanian and extending westward. Notably, the observed increases in many areas exceed the prescribed SLR values, indicating that dynamic ocean responses contribute to the amplification of sea level changes beyond the static rise alone. The spatial distribution

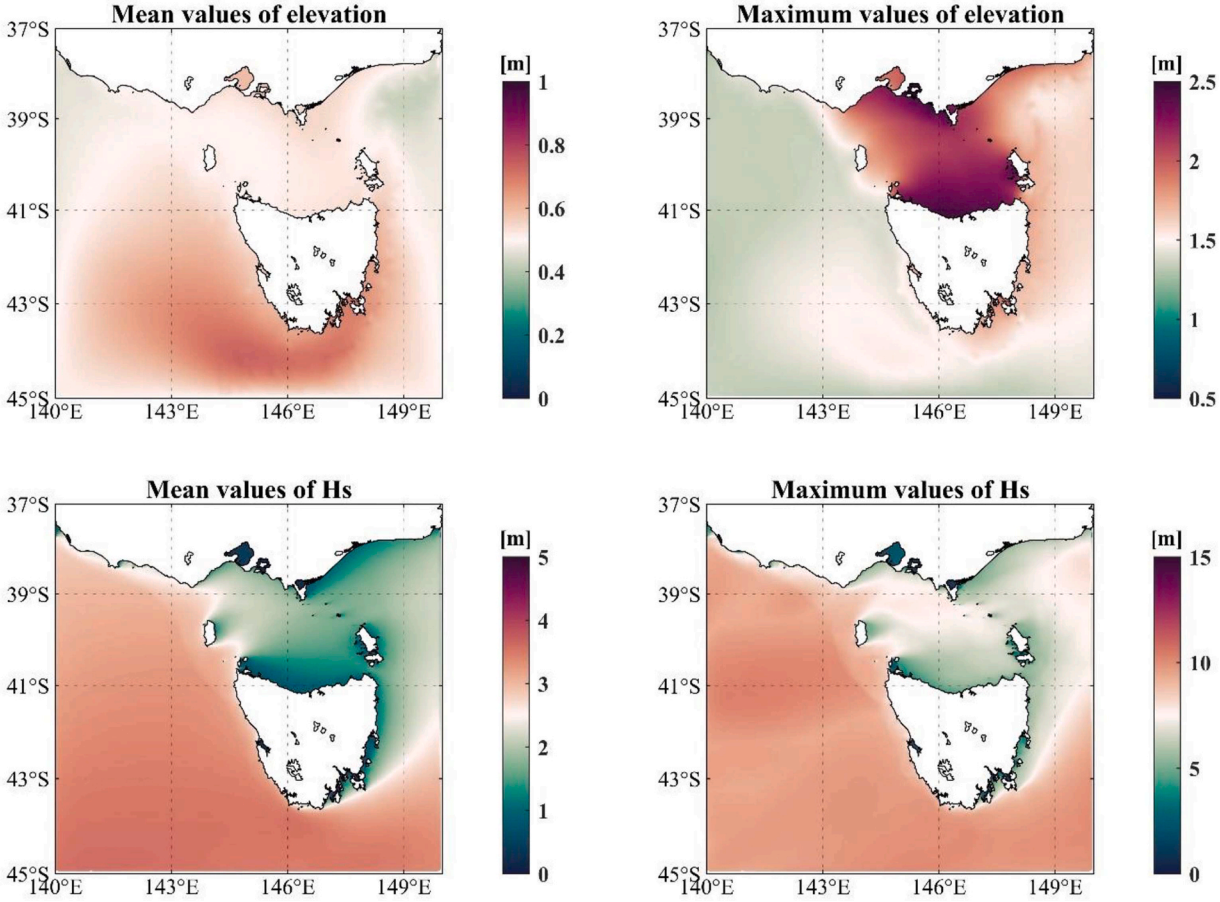

Fig. 10. Maximum and mean values of elevation and SWH over the 31-year period, considering a 0.5-meter SLR.

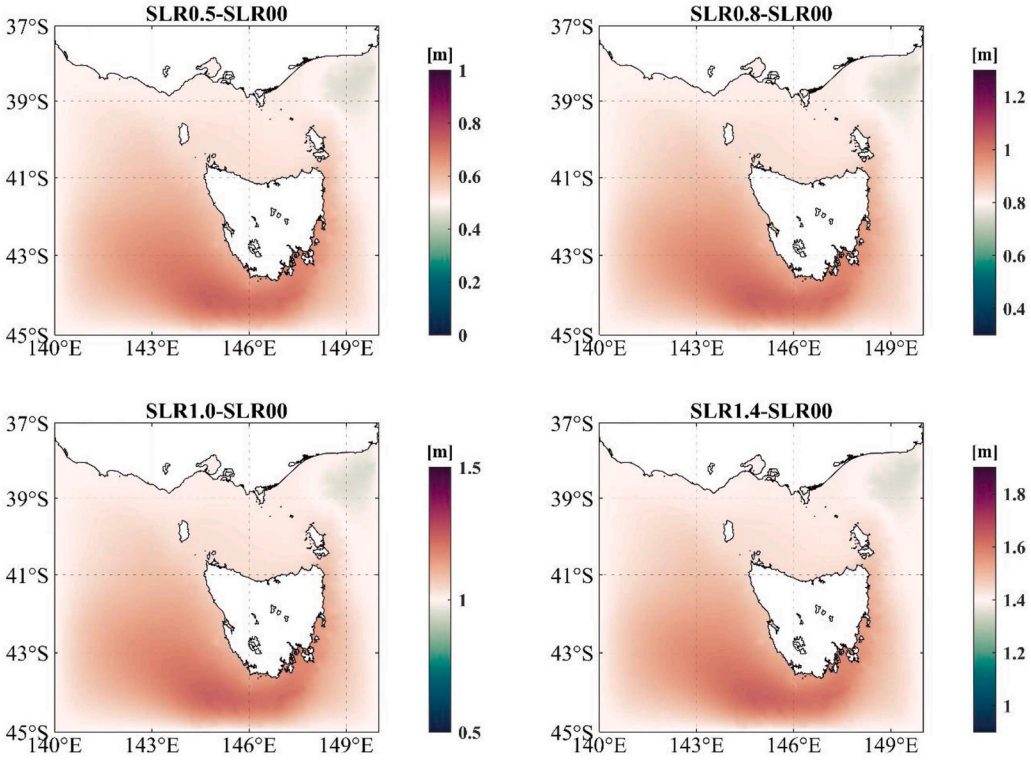

Fig. 11. Differences in mean elevation between SLR scenarios and the current conditions.

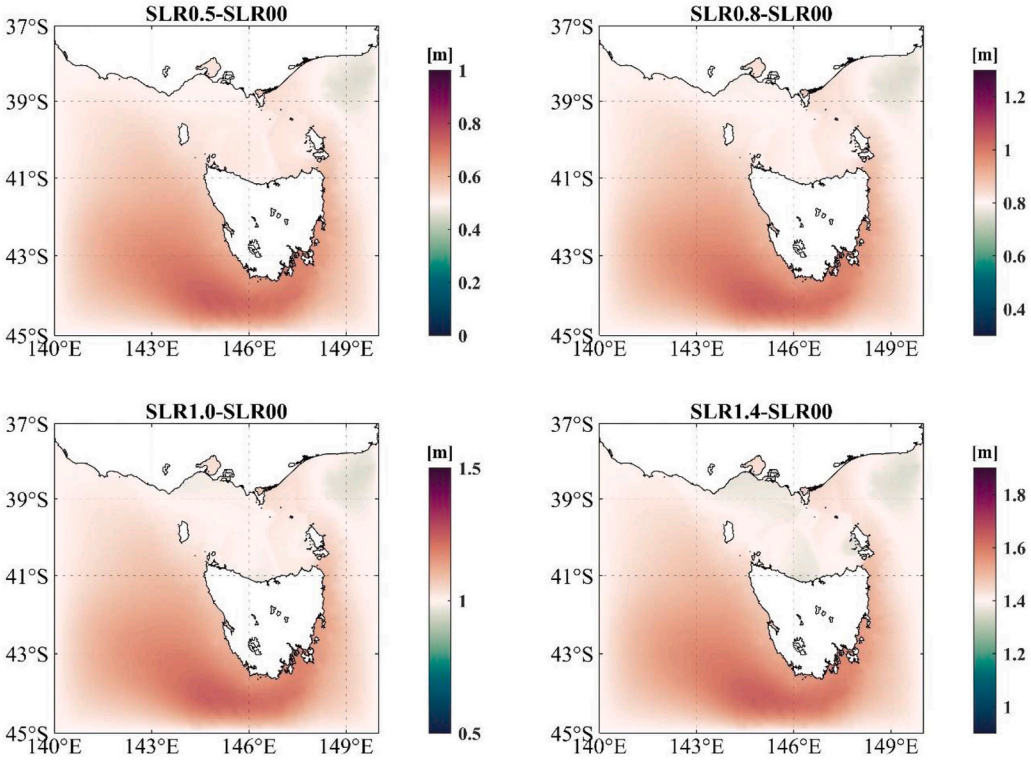

Fig. 12. Differences in maximum elevation between SLR scenario and the current conditions.

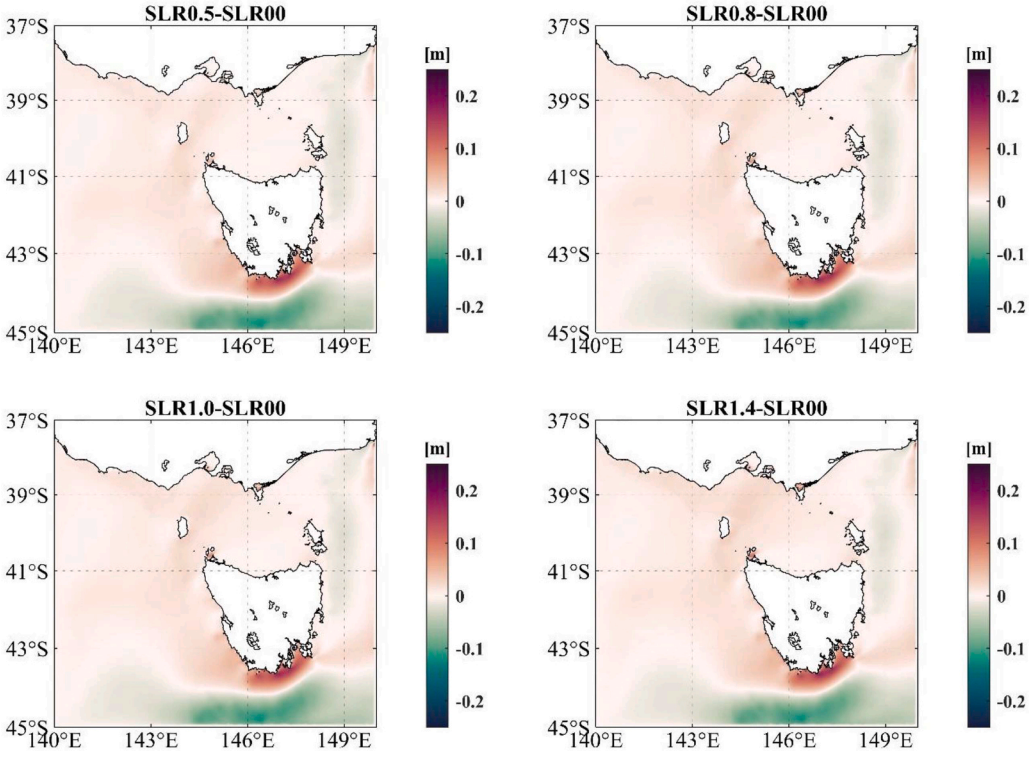

Fig. 13. Differences in mean SWH between the SLR scenarios and the current conditions.

of maximum water elevation exhibits a similar pattern with mean elevation (Fig. 12). SLR appears to have little impact on changes in extreme elevation.

Based on Figs. 13 and 14, both mean and extreme SWH exhibit similar spatial distribution patterns under SLR scenarios. In nearshore regions—particularly along southeastern Australia and around Tasmania—SWH generally increases. Under the 1.0-meter SLR scenario, maximum SWH increases by approximately 0.2 m south of Tasmania, indicating a potential shift in wave energy distribution due to altered water depths. In contrast, some deep-water areas in the Southern Ocean,

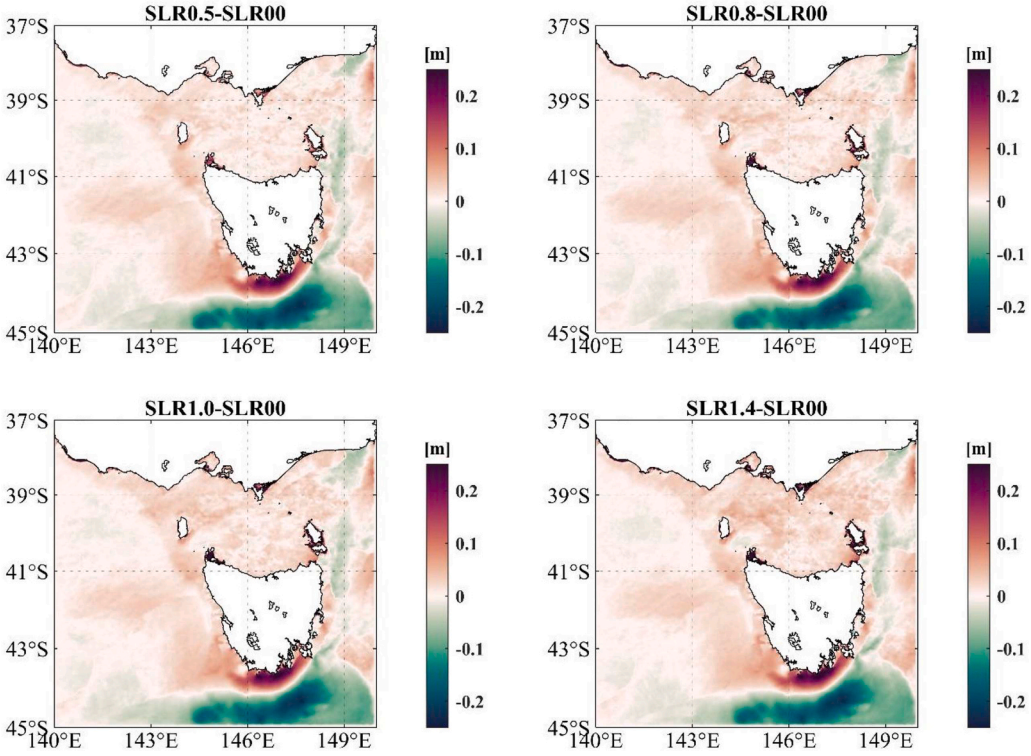

Fig. 14. Differences in maximum SWH between the SLR scenarios and the current conditions.

especially south of Tasmania, show a reduction in SWH. This decline suggests that increased water depths under SLR conditions may reduce wave breaking and dissipation, thereby affecting the transfer of wave energy. Importantly, the differences in SWH between SLR scenarios are relatively small, reflecting the non-linear nature of wave dynamics—where deeper water does not necessarily result in proportionally higher SWH. While mean and extreme SWH share the same spatial variability, the magnitude of change is more pronounced for extreme values. That is, in regions where SWH increases, the rise in extreme SWH is larger than that in mean SWH; similarly, where SWH

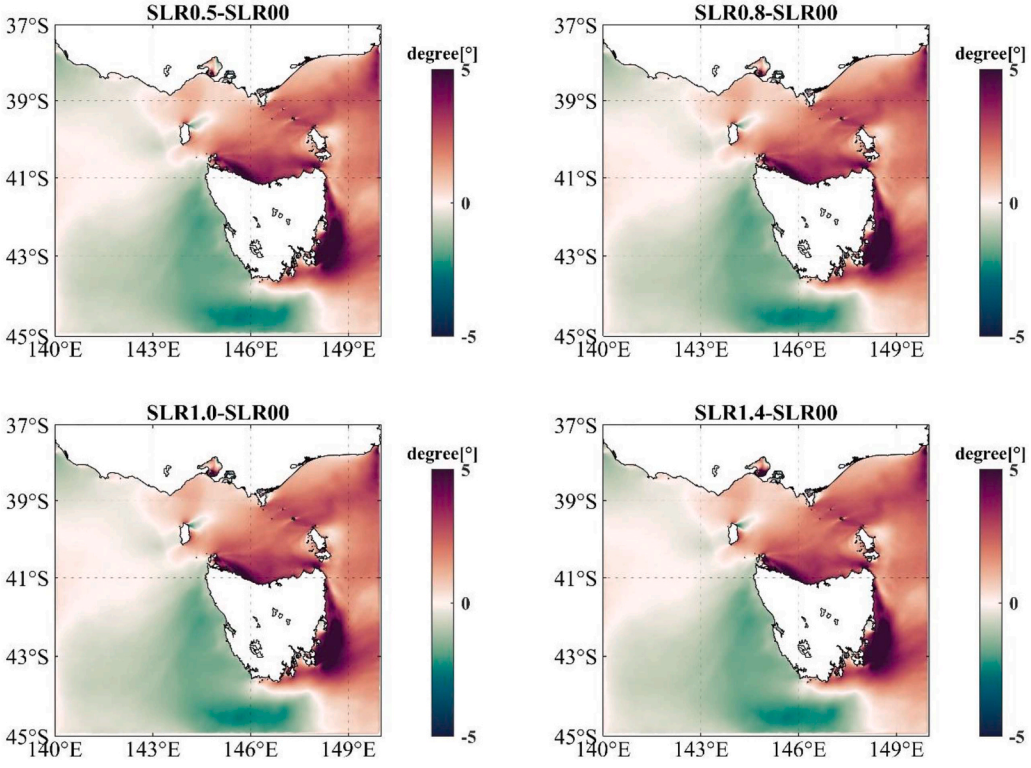

Fig. 15. Differences in mean wave direction between the SLR scenarios and the current conditions.

decrease, extreme SWH values show a greater decline. These findings highlight that although SLR tends to elevate water levels overall, its impact on SWH is spatially heterogeneous and strongly influenced by local bathymetry, wind patterns, and wave propagation dynamics. In most nearshore areas along the Victorian coast, a noticeable increase in SWH can be observed as waves propagate shoreward. Additionally, a distinct band of SWH reduction is evident in the eastern part of the study area, aligned roughly along 149°E longitude. This pattern is suspected to be influenced by ocean currents; however, further investigation and targeted experiments are needed to confirm this hypothesis.

The impacts of SLR on mean wave direction and extreme peak period were also examined in this study, as shown in Figs. 15 and 16. Changes in wave direction due to SLR are primarily concentrated east of the Bass Strait, where wave directions are deflected by approximately 4° as a result of obstructions from islands and coastal topography. Noticeable shifts in wave direction are also observed nearshore, particularly off the eastern and northern coasts of Tasmania. However, overall, SLR does not lead to significant directional changes in wave propagation. As for extreme peak period, the influence of SLR is similarly limited. In general, SLR leads to a slight increase of about 1 s in the extreme peak period, without any notable reductions. These changes are minimal and can be considered negligible in most practical applications.

5. Conclusion and discussion

This study employed the coupled wave-hydrodynamic model SCHISM-WWMIII to investigate extreme water levels and wave dynamics along southeastern Australia's coast. The model was calibrated and validated using observational data from tide gauges and wave buoys, achieving high correlations (above 0.9) between model results and measured elevation and SWH. A 31-year hindcast simulation was conducted to analyze long-term trends in water level and wave variations. The results show a rise trend in both water levels and SWH. The analysis of existing extreme water levels and wave patterns shows that high water levels are strongly influenced by storm surges and local wind forcing, with Western Port Bay exhibiting maximum elevations exceeding 2 m Wave conditions in the region are predominantly shaped by Southern Ocean swells, with extreme wave events being more frequent and intense in the waters south of Tasmania. These baseline characteristics provide a crucial reference for assessing the impacts of future SLR on coastal hydrodynamics.

The study examined the effects of SLR on water elevation and SWH, revealing that water level changes are more pronounced than SWH variations. Under SLR scenarios, most areas experience continued increases in mean and maximum water levels, with the most significant increases occurring south of Tasmania, where maximum elevation increases exceed 1.2 m under the 1.0-meter SLR scenario. Although a uniform SLR was applied at the model's open boundary, the results show notable spatial variability in elevation increases within the domain. This spatial variation is largely driven by dynamic ocean processes rather than by the external boundary forcing itself. Specifically, tidal amplification plays a critical role in redistributing the additional water mass: as tidal waves propagate into shallower waters and narrower coastal embayment, their amplitude can increase due to geometric convergence, shallow water effects, and resonance phenomena. Additionally, nonlinear hydrodynamic interactions further modify elevation near the coast, as SLR changes the local water depth and influences tidal and wave dynamics. These results highlight the importance of using fully coupled hydrodynamic–wave models to capture these complex, localized responses, as spatially uniform SLR scenarios can result in non-uniform impacts on coastal elevations due to inherent coastal dynamics.

In contrast, SWH changes exhibit spatial heterogeneity: nearshore areas generally see increased SWH, while offshore regions, particularly in the Southern Ocean, experience reductions. However, the impact of SLR on wave direction and extreme peak period is minimal, as these variables are primarily governed by wind forcing and swell conditions rather than sea level. These findings highlight the complex interactions between rising sea levels and wave dynamics, reinforcing the need for localized assessments to accurately evaluate coastal risks under future climate scenarios.

In this study, we used the past 31 years of forcing data to drive the model and investigate the effects of SLR. The four SLR scenarios applied

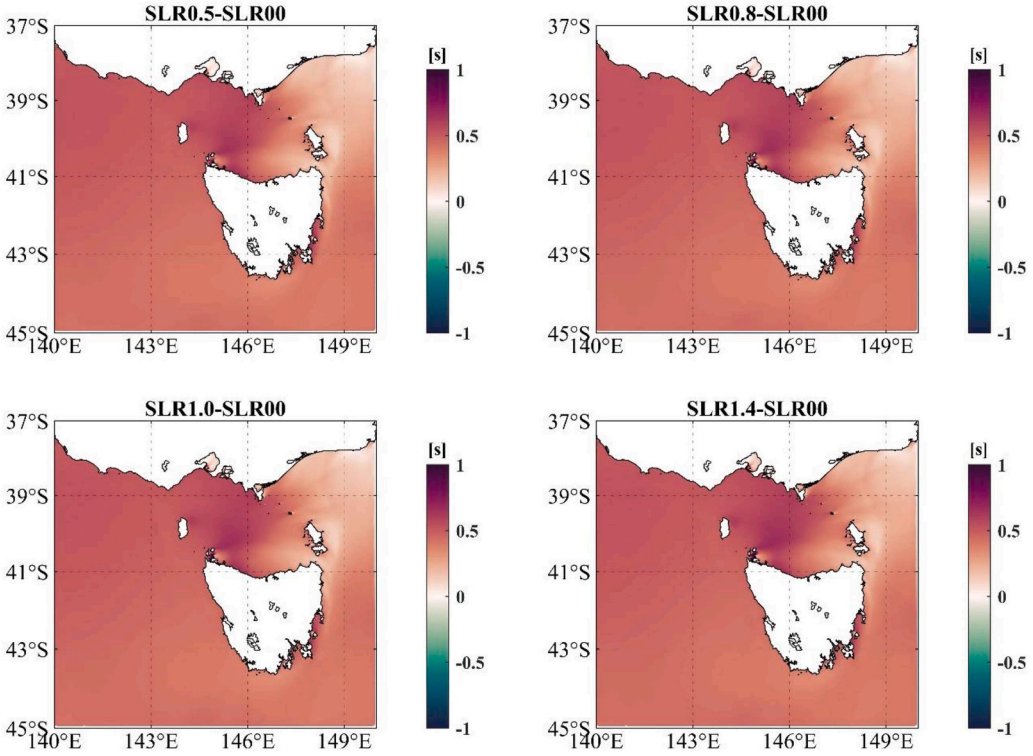

Fig. 16. Differences in mean peak period between the SLR scenarios and the current conditions.

identical forcing fields. However, in reality, future SLR may be accompanied by changes in wave conditions and atmospheric forcing. Due to data and model limitations, we were unable to obtain the necessary future climate-forced fields for the simulations. Therefore, the results presented here do not represent future nearshore hydrodynamic conditions under climate change, but rather isolate and evaluate the impact of rising sea levels alone. Furthermore, sediment transport and shoreline evolution play crucial roles in shaping coastal hydrodynamics and influencing long-term coastal change. Incorporating these processes into future research will provide a more comprehensive understanding of how coasts respond to SLR. These findings offer valuable insights for coastal management and resilience planning, supporting the development of adaptive strategies to mitigate the impacts of future SLR on coastal infrastructure, ecosystems, and communities. What's more, this study focuses on the separate impacts of SLR on mean and extreme water levels and SWH. A key limitation is that the boundary conditions do not include non-tidal residuals or background large-scale ocean currents, such as storm surges or interannual variability, which can influence coastal water levels. Additionally, our analysis presents water levels and wave heights separately; in reality, these variables may co-vary during extreme events (e.g., storm surges coinciding with high waves), potentially amplifying coastal hazards. Quantifying such compound events and joint probabilities remains an important area of ongoing research and is beyond the scope of this study. Future work could incorporate dynamically coupled surge-wave models and non-tidal residuals to assess these interactions more comprehensively.

Data availability

This study uses the global finite element solution tide model (FES 2014) developed by AVISO (Carrère et al. 2015) to specify water level variations at the open boundary. It can be downloaded from https://www.aviso.altimetry.fr/en/home.html. Atmospheric forcing inputs for the SCHISM-WWM model were sourced from ERA5 reanalysis data (Hersbach et al. 2020). The ERA5 hourly reanalysis data can be downloaded from https://cds.climate.copernicus.eu/datasets/reanalysis-era5-single-levels?tab=overview. This study utilizes WW3 hindcast data from a wave hindcast conducted by the University of Melbourne (Liu et al. 2021). The Australian National Collection of Homogenised Observations of Relative Sea Level (ANCHORS) is a national sea level dataset based on tide gauge records across Australia (Hague et al. 2022). The observed data can be downloaded from https://geonetwork.nci.org.au/geonetwork/srv/eng/catalog.search#/metadata/f2262_2926_6911_5843.

CRediT authorship contribution statement

Rui Li: Writing – review & editing, Writing – original draft, Visualization, Validation, Software, Formal analysis, Data curation. **Huy Quang Tran:** Software, Methodology. **Jak McCarroll:** Writing – review & editing. **Alexander V. Babanin:** Writing – review & editing, Supervision.

Declaration of competing interest

The authors declare that they have no known competing financial interests or personal relationships that could have appeared to influence the work reported in this paper.

Acknowledgments

The author(s) declare financial support was received for the research, authorship, and/or publication of this article. This project was supported by the grant of Department of Energy, Environment and Climate Action (DEECA) of the Government of Victoria. This research was also supported by the University of Melbourne Research Computing Services. Rui Li also acknowledges the National Key Research and Development Program of China (2022YFC3105002 and 2023YFC3107803) and the support from the National Natural Science Foundation of China under grant numbers 42176018 and 41976017.

References

Anghel, C.G., 2024. Revisiting the use of the gumbel distribution: a comprehensive statistical analysis regarding modeling extremes and rare events. Mathematics 12.
Arns, A., and Coauthors, 2020: Non-linear interaction modulates global extreme sea levels, coastal flood exposure, and impacts, 11.
Bhaskaran, P.K., Neelamani, S., Al-Salem, K., Krishnan, A., Albert, J., Sreelakshmi, S., 2022. Extreme wind-wave characteristics in the north indian ocean in a changing climate. In: Unnikrishnan, A.S., Tangang, F., Durrheim, R.J. (Eds.), Extreme Natural Events: Sustainable Solutions For Developing Countries. Springer Nature, Singapore, pp. 223–280.
Carrère, L., F.H. Lyard, M. Cancet, and A. Guillot, 2015: FES 2014, a new tidal model on the global ocean with enhanced accuracy in shallow seas and in the Arctic region.
Coles, S., 2001. An Introduction to Statistical Modeling of Extreme Values, 97. Springer, p. 1204. - 1204.
Dodet, G., Melet, A., Ardhuin, F., Bertin, X., Idier, D., Almar, R., 2019. The contribution of wind-generated waves to coastal sea-level changes. Surv. Geophys. 40, 1563–1601.
Dong, X., Coauthors, 2025. Numerical simulations of ocean surface waves along the Australian coast with a focus on the Great Barrier Reef. EGUsphere 2025, 1–31.
Ercelebi, S.G., Toros, H., 2009. Extreme value analysis of istanbul air pollution data. CLEAN - Soil Air Water 37, 122–131.
Fisher, R.A., Tippett, L.H.C., 1928. Limiting forms of the frequency distribution of the largest or smallest member of a sample. Math. Proc. Camb. Philos. Soc. 24, 180–190.
Guérin, T., Bertin, X., Coulombier, T., de Bakker, A., 2018. Impacts of wave-induced circulation in the surf zone on wave setup. Ocean Model. 123, 86–97.
Hague, B.S., Jones, D.A., Trewin, B., Jakob, D., Murphy, B.F., Martin, D.J., Braganza, K., 2022. ANCHORS: a multi-decadal tide gauge dataset to monitor Australian relative sea level changes. Geosci. Data J. 9, 256–272.
Hernaman, V., Hoeke, R.K., McInnes, K.L., O'Grady, J.G., Couto, P.P., Trenham, C., Seers, B.M., 2025. The effect of sea-level rise on tides, extreme sea levels and waves in Port Phillip Bay in south-eastern Australia. Ocean Model. 196.
Hersbach, H., Coauthors, 2020. The ERA5 global reanalysis. Q. J. R. Meteorol. Soc. 146, 1999–2049.
Ierodiaconou, D., Coauthors, 2022. Citizen science unoccupied aerial vehicles: a technique for advancing coastal data acquisition for management and research. Cont. Shelf Res. 244, 104800.
Jain, R.K., 2011. Entrepreneurial competencies: a meta-analysis and comprehensive conceptualization for future research. Vision 15, 127–152.
Jenkinson, A.F., 1955. The frequency distribution of the annual maximum (or minimum) values of meteorological elements. Q. J. R. Meteorol. Soc. 81, 158–171.
Kang, D., Ko, K., Huh, J., 2015. Determination of extreme wind values using the Gumbel distribution. Energy 86, 51–58.
Kochanek, K., Renard, B., Arnaud, P., Aubert, Y., Lang, M., Cipriani, T., Sauquet, E., 2014. A data-based comparison of flood frequency analysis methods used in France. Nat. Hazards Earth Syst. Sci. 14, 295–308.
Li, R., Wu, K., Li, J., Akhter, S., Dong, X., Sun, J., Cao, T., 2021. Large-scale signals in the South Pacific wave fields related to ENSO. J. Geophys. Res.: Oceans 126.
Li, R., Wu, K., Li, J., Dong, X., Sun, J., Zhang, W., Liu, Q., 2022. Relating a large-scale variation of waves in the indian ocean to the IOD. J. Geophys. Res.: Oceans 127.
Li, R., Coauthors, 2023. Analysis of the 20-year variability of ocean wave hazards in the northwest pacific. Remote Sens. 15.
Liu, J., Meucci, A., Liu, Q., Babanin, A.V., Ierodiaconou, D., Xu, X., Young, I.R., 2023. A high-resolution wave energy assessment of south-east Australia based on a 40-year hindcast. Renew. Energy 215.
Liu, Q., Coauthors, 2019. Observation-based source terms in the third-generation wave model Wavewatch III: updates and verification. J. Phys. Oceanogr. 49, 489–517.
Liu, Q., Coauthors, 2021. Global wave hindcasts using the observation-based source terms: description and validation. J. Adv. Model. Earth Syst. 13, e2021MS002493.
Lyddon, C.E., Brown, J.M., Leonardi, N., Plater, A.J., 2019. Increased coastal wave hazard generated by differential wind and wave direction in hyper-tidal estuaries. Estuar. Coast. Shelf Sci. 220, 131–141.
McInnes, K.L., O'Grady, J., Macadam, I., 2009a. The effect of climate change on extreme sea levels in Port Phillip Bay. CSIRO Mar. Atmos. Res 1–58.
McInnes, K.L., Macadam, I., Hubbert, G.D., O'Grady, J.G., 2009b. A modelling approach for estimating the frequency of sea level extremes and the impact of climate change in southeast Australia. Nat. Hazards 51, 115–137.
McInnes, K.L., Macadam, I., Hubbert, G., O'Grady, J., 2013. An assessment of current and future vulnerability to coastal inundation due to sea-level extremes in Victoria, southeast Australia. Int. J. Climatol. 33, 33–47.
McInnes, K.L., O'Grady, J.O., Prakash, M., Dahlhaus, P., Rosengren, N.J., Hoeke, R.K., Lauchlan Arrowsmith, C., Hernaman, V., Cohen, R., Seers, B., Chen, Y., Walters, D., Couto, P., Trenham, C., Forbes-Smith, N. Gregory, R., Hemer, M. and Power, R., 2022: Port Phillip Bay Coastal Hazard Assessment: final Report, 236 pages + 211 Appendices. pp.
Meucci, A., Young, I.R., Aarnes, O.J., Breivik, Ø., 2020. Comparison of wind speed and wave height trends from twentieth-century models and satellite altimeters. J. J. Clim. 33, 611–624.

Morim, J., Cartwright, N., Etemad-Shahidi, A., Strauss, D., Hemer, M., 2016. Wave energy resource assessment along the Southeast coast of Australia on the basis of a 31-year hindcast. Appl. Energy 184, 276–297.
Pryor, S.C., Barthelmie, R.J., 2021. A global assessment of extreme wind speeds for wind energy applications. Nat. Energy 6, 268–276.
Rogers, W.E., Babanin, A.V., Wang, D.W., 2012. Observation-consistent input and whitecapping dissipation in a model for wind-generated surface waves: description and simple calculations. J. Atmos. Ocean. Technol. 29, 1329–1346.
Roland, A., 2008: Development of WWM II: spectral wave modeling on unstructured meshes.
Roland, A., Coauthors, 2012. A fully coupled 3D wave-current interaction model on unstructured grids. J. Geophys. Res.: Oceans 117.
Sharmar, V.D., M.Y. Markina, and S.K. Gulev, 2021: Global ocean wind-wave model hindcasts forced by different reanalyzes: a comparative assessment, 126, e2020JC016710.
Tolman, H.L., 1992. Effects of numerics on the physics in a third-generation wind-wave model. J. Phys. Oceanogr. 22, 1095–1111.
Tran, H., 2020. Hydrodynamic Modelling of a Wave-Dominated Tidal Inlet System. Port Phillip Bay, Australia.
Tran, H., R. McCarroll, and A. Babanin, 2023: *Improvement of Port Philip Bay coupled hydrodynamic hindcast model.*
Tran, H.Q., Cruz, F.A., McCarroll, J., Babanin, A., 2024. Non-linear surges and extreme wind-waves in Port Phillip Bay under existing and future mean sea levels. Front. Mar. Sci. 11, 1480054.
Wahl, T., Haigh, I.D., Nicholls, R.J., Arns, A., Dangendorf, S., Hinkel, J., Slangen, A.B.A., 2017. Understanding extreme sea levels for broad-scale coastal impact and adaptation analysis. Nat. Commun. 8, 16075.
Woo, H.-J., Park, K.-A., 2021. Estimation of extreme significant wave height in the northwest pacific using satellite altimeter data focused on typhoons (1992–2016). Remote Sens. 13.
Wright, L.D., Caruson, K., Elia, C.D., Draayer, J., Nichols, R., Weiss, R., Zarillo, G., 2020. Assessing and planning for the impacts of storms, flooding and sea level rise on vulnerable gulf of mexico coastal communities: a white paper. Glob. Oceans 2020: Singap. – U.S. Gulf Coast 1–6.
Young, I.R., Ribal, A., 2019. Multiplatform evaluation of global trends in wind speed and wave height. Science 364, 548–552.
Young, I.R., Zieger, S., Babanin, A.V., 2011. Global trends in wind speed and wave height. Science 332, 451–455.
Zhang, W.Q., Li, R., Zhu, D.L., Zhao, D.L., Guan, C.L., 2023a. An investigation of impacts of surface waves-induced mixing on the upper ocean under typhoon megi (2010). Remote Sens. 15, 1862.
Zhang, W.Q., Zhang, J.L., Liu, Q.X., Sun, J., Li, R., Guan, C.L., 2023b. Effects of surface wave-induced mixing and wave-affected exchange coefficients on tropical cyclones. Remote Sens. 15, 1594.
Zhang, X., Coauthors, 2023c. Analysis of the interannual variability of pacific swell pools. J. Mar. Sci. Eng. 11.
Zhang, Y., Baptista, A.M., 2008. SELFE: a semi-implicit Eulerian–Lagrangian finite-element model for cross-scale ocean circulation. Ocean Model. 21, 71–96.
Zhang, Y.J., F., Ye, Stanev, E.V., Grashorn, S., 2016. Seamless cross-scale modeling with SCHISM. Ocean Model. 102, 64–81.